

Keypoints Detection in RGB-D Space

A Hybrid Approach

Nizar Sallem¹, Michel Devy¹, Suat Gedikili² and Radu Rusu³

¹LAAS-CNRS, Université de Toulouse, Toulouse, France

²Willow Garage, Menlo Park, CA, U.S.A.

³Open Perception, Menlo Park, CA, U.S.A

Keywords: Keypoints, Corner, Detection, RGB-D.

Abstract: Features detection is an important technique of image processing which aim is to find a subset, often discrete, of a query image satisfying uniqueness and discrimination criteria so that an image can be abstracted to the computed features. Detected features are then used in video indexing, registration, object and scene reconstruction, structure from motion, etc. In this article we discuss the definition and implementation of such features in the RGB-Depth space **RGB-D**. We focus on the corners as they are the most used features in image processing. We show the advantage of using 3D data over image only techniques and the power of combining geometric and colorimetric information to find corners in a scene.

1 INTRODUCTION

Corner detection in images can be traced back to Moravec (Moravec, 1981) who used small pixel neighborhood (patches) to define a region of an image as an edge or a corner comparing it to its surrounding regions. Followed by Harris and Stephens, Plessey and Shi-Tomasi who overcome the slowness of Moravec's detector using the image's second moment matrix to account for intensity direction change and thus corner presence. A considerable amount of work was achieved toward invariance in scale and affine transformation leading to robust features. A detailed review of keypoint detectors can be found in (Tuytelaars and Mikolajczyk, 2008) and (Li and Allinson, 2008). When they rely on intensity changes, corners behave poorly in texture-less environment and bad light conditions. Geometric data, on the other hand is not sensitive to such arguments, and a geometric based corner detector should behave equally regardless to the presence or absence of texture under different light conditions. We propose an extension to popular image corner detector where we account for geometric changes to define the cornerness measure that we enhance further by integrating intensity information.

Detecting corners in a 3D point cloud is a challenging, relatively new topic in computer vision. In (Sipiran and Bustos, 2011) authors address the problem of detecting corners in a 3D mesh. They exploit

the mesh connectivity for local information and use PCA to tear down the problem and exploit directly the 2D algorithm in (Harris and Stephens, 1988). In (Knopp et al., 2010) and (Redondo-Cabrera et al., 2012), authors detect 3D SURF corners exploiting mesh and voxel grid. They first voxelize the shape into a 256^3 voxel grid using faces intersection with grid edges then they apply the algorithm in (Bay et al., 2006) accounting for one additional dimension.

Compared to these work we also address the problem of finding corners in 3D but we choose to rely also on geometric data to discriminate corners from regular points not only intensity as in all the above mentioned references. An additional difference with (Sipiran and Bustos, 2011) and (Knopp et al., 2010) is that we perform detection on the points at an earlier stage of the acquisition pipeline with no shape nor mesh information which saves time and resources. Furthermore, we don't require voxelization which is an expensive technique and rely solely on local information.

In section 2 we extend intensity based corners to 3D. Combination of geometric and color criteria is done in 3. The results of novel detectors are the subject of the evaluation in 4.

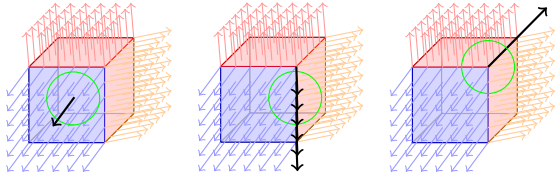


Figure 1: Normal direction at different point locations within its local neighborhood (green circle). a. point on a plane b. point on an edge c. point on a corner.

2 CORNER DETECTION IN 3D

Observation of the normals at 3D points locations lead to:

1. if point (p_0, \vec{n}_0) is on a plane then all the normals \vec{n}_i in a sufficiently small neighborhood are parallel;
2. if point (p_0, \vec{n}_0) is on an edge e , the neighborhood is divided on three distinct groups: points on the edge share same normal direction as \vec{n}_0 and points on both sides of e have respectively two directions Δ^+ and Δ^- ;
3. if point is a corner or an isolated point then immediate neighbors would have distinct normals directions.

These situations are illustrated on Figure 1. Variation in normals directions appears to be a good indicator on corner presence. We can separate the detectors in two families according to how it is computed: second order moments and self dissimilarity.

2.1 Self Dissimilarity Detectors

A natural way to compute the variation is to account the differences between the central pixel, *nucleus*, value and its neighbors. Smallest Univalued Segment Assimilating Nucleus (SUSAN) (Smith and Brady, 1995) and Minimum Intensity Change (MIC) (Trajkovic and Hedley, 1998) detectors rely on this principle in a more elaborated way to find corners on an image. When dealing with normals the angle formed by normals direction is a good indicator on normals differences.

For the extended SUSAN version, a spherical mask M is placed on the nucleus n and

$$\forall p \in M, c(p) = N(p) \cdot N(n) \quad (1)$$

Then M_c is computed as

$$M_c(n) = \begin{cases} g - A(n) = g - \sum_{p \in M} c(p), & A(n) < g \\ 0 & \text{else} \end{cases} \quad (2)$$

The extended MIC on the other hand is stated as:

$$\forall p \in M, c(p) = (N(p) \cdot N(n))^2 + (N(p') \cdot N(n))^2 \quad (3)$$

where (p, p') are diametrically opposed with respect to n . Then

$$M_c(n) = \min_{p \in M} (c(p)) \quad (4)$$

2.2 Second Order Moments Matrix Detectors

Consider a point cloud P with normals N , the sum S of the squared differences of a patch around region defined by (u, v, w) of P shifted by an amount (x, y, z) is given in Equation 5. We exploit Taylor's expansion as in (Harris and Stephens, 1988): $N(u+x, v+y, w+z) \approx N(u, v, w) + N_x(u, v, w)x + N_y(u, v, w)y + N_z(u, v, w)z$ where N_x, N_y and N_z , respectively, are the components along X, Y and Z axis of normal N .

\mathcal{A} in Equation 5 corresponds to normals covariance matrix and its eigenvalues $(\lambda_1, \lambda_2, \lambda_3)$ analysis offers a clear indication on the direction of variations.

- Harris: $\mathcal{M}_c = \lambda_1 \lambda_2 \lambda_3 - \kappa (\lambda_1 + \lambda_2 + \lambda_3)^2 = \det(\mathcal{A}) - \kappa \text{trace}^2(\mathcal{A})$, κ a tunable parameter;
- Shi-Thomasi: $\mathcal{M}_c = \min(\lambda_1, \lambda_2, \lambda_3)$;
- Noble: $\mathcal{M}_c = \det(\mathcal{A}) / \text{trace}(\mathcal{A})$;
- Lowe: $\mathcal{M}_c = \det(\mathcal{A}) / (\text{trace}(\mathcal{A}))^2$.

3 HYBRID DETECTION IN RGB-D

From the observations in Section 2, a problem shows up concerning the proposed algorithms when dealing with superposed planar objects or coplanar planar objects. Indeed, since the normals are parallel no difference can be computed so no corners will be detected. We can take advantage of the RGB-D sensors to discriminate corners either according to geometric criterion when they are located on different planes even if they have the same intensity value or with help of intensity if they have different textures.

Detection result on some objects in the RGB-D dataset (Lai et al., 2011) are shown in the Figure 2 and . Note that due to the working range of the camera, some point clouds are too small to be displayed. We used Lowe response and a search radius of $0.10 m$. We show 3D keypoints and hybrid ones to show difference in location. Same search radius $0.01 m$ is used for both hybrid and 3D detection.

$$\begin{aligned}
 S(x,y,z) &= \sum_{uvw} \left[\alpha_{uvw} [N(u+x, v+y, w+z) - N(u, v, w)]^2 \cdot N(u+x, v+y, w+z) \right] \\
 &\approx [x \ y \ z] \sum_{uvw} \alpha_{uvw} \begin{bmatrix} N_x^2 & N_x N_y & N_x N_z \\ N_y N_x & N_y^2 & N_y N_z \\ N_z N_x & N_z N_y & N_z^2 \end{bmatrix} \begin{bmatrix} x \\ y \\ z \end{bmatrix} \\
 &\approx [x \ y \ z] \mathcal{A} \begin{bmatrix} x \\ y \\ z \end{bmatrix}
 \end{aligned} \tag{5}$$



Figure 2: Hybrid keypoints on cereal boxes from the RGB-D dataset. 3D keypoints are displayed with red spheres, hybrid keypoints are displayed with green spheres. Notice that the red spheres location is different from the green ones due to the added intensity variation. First row corresponds to Harris detectors and second row to SUSAN detectors.

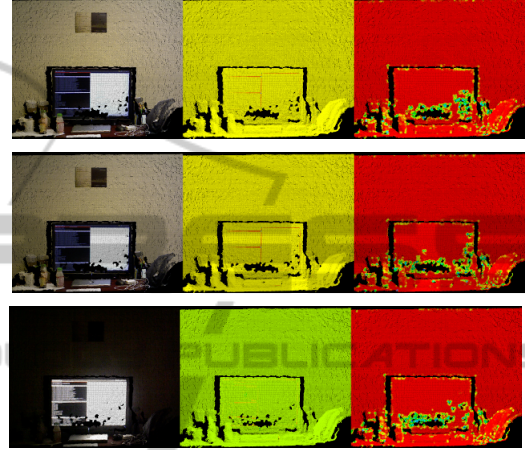


Figure 3: Geometric detectors evaluation: light invariance. Scene images (left column) were acquired using an **Asus Xtion PRO LIVE** RGB-D camera. Image corners detection (middle column) was performed using a window of size 3×3 . Geometric corners detection (right column) was performed using a radius $0.015m$. Cornerness is displayed from red (low) to green (high). The 2D response fades as the light is dimmed.

4 EXPERIMENTAL RESULTS

Two major limitations of the classic corner detector we address are the light conditions and the absence of texture. In here, we evaluate performance of the geometric or 3D corner detector in such situations. To achieve a fair comparison we use a RGB-D sensor that outputs 3D and images data. Geometric detectors are evaluated against their images homologous in different illumination and texture conditions.

4.1 Light Invariance

For this experiment we take 3 images of the same scene with different lighting conditions. We compare corners detection with Harris method on the 3D point cloud and the image. As shown on the Figure 3, 3D corners are more stable to light conditions.

Repeatability of the detectors can be evaluated for the above mentioned dataset by comparing the 3D responses:

$$\bar{\epsilon}_{3D} = \frac{\sum \delta_{3D}(p_i)}{card(P_1)}, \delta_{3D}(p_i) = M_c(P_1(p_i)) - M_c(P_2(p_i))$$

and 2D ones:

$$\bar{\epsilon}_{2D} = \frac{\sum \delta_{2D}(p_i)}{card(I_1)}, \delta_{2D}(p_i) = M_c(I_1(p_i)) - M_c(I_2(p_i))$$

for all available pairs. $\bar{\epsilon}_{3D}$ is the 3D repeatability mean error of standard deviation σ_{3D} and its counterpart $\bar{\epsilon}_{2D}$ of standard deviation σ_{2D} . $\bar{\epsilon}_{3D} = 0$ which proves the stability of the 3D corner detector in strong light variation while $\bar{\epsilon}_{2D}$ varies significantly. Table 1 sums up these results.

4.2 Texture Invariance

To evaluate the performance of the 3D corners on texture, we acquired a data set of objects with similar shapes but carrying different textures (text, colors, pictures). We measure the cornerness using intensity

Table 1: Corners repeatability mean and standard error deviation in strong light variation for 2D and 3D Harris corner detectors. $P_{i1 \leq i \leq 3}$ are the input clouds. The mean error $\bar{\epsilon}_{2D}$ high values show how light affects 2D corners.

<i>pairs</i>	$P_1 - P_2$	$P_1 - P_3$	$P_2 - P_3$
$\bar{\epsilon}_{2D}$	177034	695510	698783
$\bar{\epsilon}_{3D}$	0	0	0
σ_{2D}	$1.54e+06$	$5.42e+06$	$5.81e+06$
σ_{3D}	0	0	0

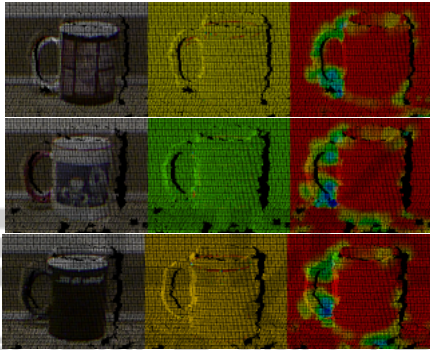


Figure 4: Geometric corners detection: texture invariance. Cornerness is displayed from green (weak) to red (strong). 3D cornerness - right column - is almost the same for all the objects although they carry different textures while 2D cornerness - middle column - varies according to the texture.

and normals. Detection results (non filtered) are presented in Figure 4.

The results shown on Figure 4, confirm our intuition: since we rely solely on geometric data variation for this experiment, objects of the same shape should have similar signature. Lecturers can easily notice that 3D cornerness measure is analogous for the whole 3rd column while it differs depending on the object texture along the 2nd column.

5 CONCLUSIONS

This paper addresses the problem of corner detection in RGB-D space to improve repeatability under strong light variation or in texture-less environments. The novelty of the proposed solution is the use of a geometric criterion to assess the nature of a point. The novel detectors are extension of popular 2D images corner detectors: second moment matrix and self-discriminability ones. We prove stability of designed detectors through experimental validation. Future work include application to point cloud registration, object recognition and tracking.

ACKNOWLEDGMENTS

This work has been supported both by the French national research agency (ANR) by the project ANR Assist ANR-07-ROBO-0011, and by the Willow Garage company, Menlo Park, California, USA.

REFERENCES

- Bay, H., Tuytelaars, T., and Van Gool, L. (2006). Surf: Speeded up robust features. pages 404–417.
- Harris, C. and Stephens, M. (1988). A combined corner and edge detection. In *Proceedings of The Fourth Alvey Vision Conference*, pages 147–151.
- Knopp, J., Prasad, M., Willems, G., Timofte, R., and Van Gool, L. (2010). Hough transform and 3d surf for robust three dimensional classification. In *Proceedings of the 11th European conference on Computer vision: Part VI, ECCV'10*, pages 589–602, Berlin, Heidelberg. Springer-Verlag.
- Lai, K., Bo, L., Ren, X., and Fox, D. (2011). A large-scale hierarchical multi-view RGB-D object dataset. In *ICRA*, pages 1817–1824. IEEE.
- Li, J. and Allinson, N. M. (2008). A comprehensive review of current local features for computer vision. *Neurocomput.*, 71(10-12):1771–1787.
- Moravec, H. P. (1981). 3d graphics and the wave theory. In *SIGGRAPH '81: Proceedings of the 8th annual conference on Computer graphics and interactive techniques*, pages 289–296, New York, NY, USA. ACM.
- Redondo-Cabrera, C., Lopez-Sastre, R. J., Acevedo-Rodriguez, J., and Maldonado-Bascon, S. (2012). SURFing the point clouds: Selective 3D spatial pyramids for category-level object recognition. In *IEEE CVPR*.
- Sipiran, I. and Bustos, B. (2011). Harris 3d: a robust extension of the harris operator for interest point detection on 3d meshes. *Vis. Comput.*, 27(11):963–976.
- Smith, S. M. and Brady, J. M. (1995). Susan - a new approach to low level image processing. *International Journal of Computer Vision*, 23:45–78.
- Trajkovic, M. and Hedley, M. (1998). Fast corner detection. *Image Vision Comput.*, 16(2):75–87.
- Tuytelaars, T. and Mikolajczyk, K. (2008). Local invariant feature detectors: a survey. *Found. Trends. Comput. Graph. Vis.*, 3(3):177–280.